Shock and Vibration 19 (2012) 669–677
DOI 10.3233/SAV-2011-0658
IOS Press

Aerosolization of water ejected from a full container impacted by bomb fragments

Leo W. Stockham[a], Richard N. Fry, Jr.[b], Paul W. Graham[c,*] and Todd H. Pierce[d]
[a]*TASC Inc., Albuquerque, NM, USA*
[b]*Defense Threat Reduction Agency, Fort Belvoir, VA, USA*
[c]*U.S. Army Engineer Research and Development Center, 3909 Halls Ferry Road, Vicksburg, MS, USA*
[d]*SAIC Intelligence, Security and Technology Group, San Diego, CA, USA*

Received 18 May 2010
Revised 6 October 2011

Abstract. In assessing the potential collateral effects of bomb attacks on tanks of stored liquids, it is useful to separate the liquid that is aerosolized as an escaping cloud from that which remains inside the tank or rapidly falls to the nearby ground. One relationship currently in use partitions the two categories using a linear model of aerosolized fraction versus fragment energy deposited per unit mass of liquid which is based on calculations and a few test data points. Since this model is incorporated in popular programs used by an expanding number of first responders to assess potential hazards, there is a need for high-confidence test data across the parameter space of interest to improve and/or validate the model. Such a series of tests was conducted during November of 2008 in which 7.57-liter (ℓ) sized cans of water were impacted with fragments of known mass using scored cased explosive charges. Impact velocities were measured, and the remaining water in the can and on the nearby ground platform was collected and weighed. The missing water was assumed to be aerosolized. This new data establishes an S-curve as a more accurate relationship between aerosolized fraction (AF) and the fragment energy deposited per unit mass of liquid in the container.

Keywords: Collateral effects, aerosolized liquids, aerosolized clouds, chemical clouds, chemical plumes, fragment effects on liquid filled tanks, fragment rammed tanks, rammed liquid tanks, aerosolized fraction

1. Introduction

In assessing the potential collateral effects of bomb attacks on facilities containing tanks of stored liquids, studies of high speed video of the impacts of bomb fragments on such tanks suggest the adoption of a bimodal droplet model for the ejected liquid. This model separates the liquid immediately released as an aerosol or in small droplets that will quickly aerosolize and be available to propagate downwind from that which remains in the tank or is released and rapidly falls to the ground in bulk or as large drops. One relationship based on very limited test data separates the two categories using a linear model for aerosolized fraction versus energy deposited per unit mass. Since this model is currently incorporated in programs used by an expanding number of first responders to assess potential hazards, there is a need to validate it. Twenty small scale explosive tests, specifically designed to provide this required data, were conducted during November of 2008. Each test used a 7.57 ℓ (2 gal) sized can of water positioned above a steel collection surface that was impacted with fragments of known mass from scored cased explosive charges. Impact velocities were measured and combined with the fragment mass to give the kinetic energy input, and the water remaining in the can and on the steel surface collected and weighed. The missing water, the difference between the amount of water initially in the can and the total amount recovered, was assumed to be aerosolized. This paper

*Corresponding author. Tel.: +1 601 634 3166; Fax: +1 601 634 2211; E-mail: Paul.W.Graham@usace.army.mil.

ISSN 1070-9622/12/$27.50

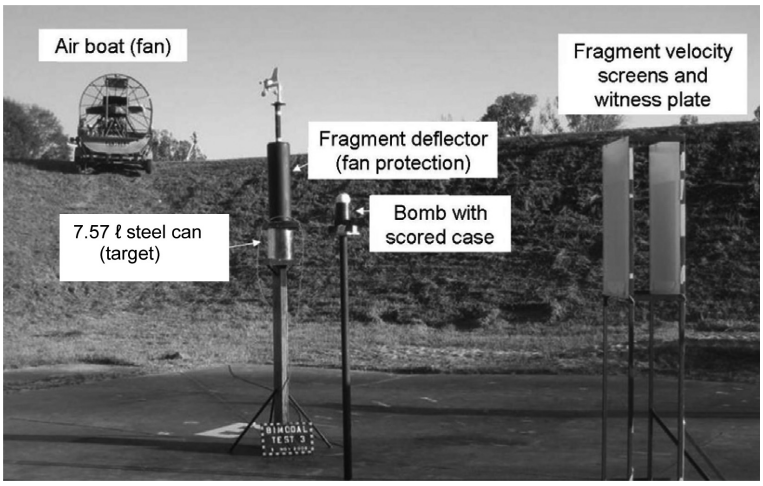

Fig. 1. Overview of the test setup.

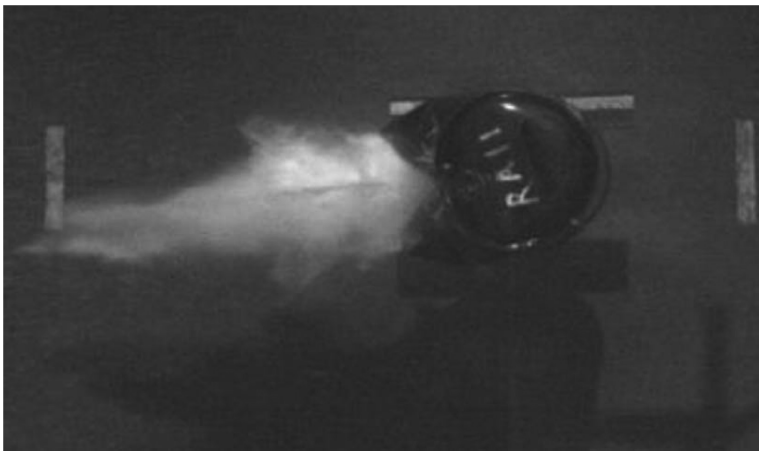

Fig. 2. Hydraulic ram (bomb location was to the left of this view).

addresses the test setup, execution and results of those tests and establishes an S-curve, instead of a straight line, as a much improved fit for the relationship between aerosolized fraction and the energy deposited per unit mass of water in the container.

This test series, sponsored by the Defense Threat Reduction Agency (DTRA), was conducted at U.S. Army Engineer Research and Development Center (ERDC) during November 2008. Technical support was provided by Science Application International Corporation (SAIC) and Northrop Grumman Information Systems (NGIS) (now TASC Inc).

2. Test setup – Overview

As shown in Fig. 1, the tests were conducted on a steel platform in a bermed basin at ERDC's Big Black Test Site (BBTS). The target cans filled with water were elevated 1.52 m (5 ft) above the platform to delay interaction with the platform surface. Scored cased charges were placed at a range of 1.83 m (6 ft) and elevated to account for the fragment drop resulting from a top initiation of the charge. Fragments from scored cases travel at known azimuths along radial paths from the charge centerline so one column of scored fragments was aimed at the target can. Fragment velocity screens and a witness plate were positioned to intercept a second fragment column. Since

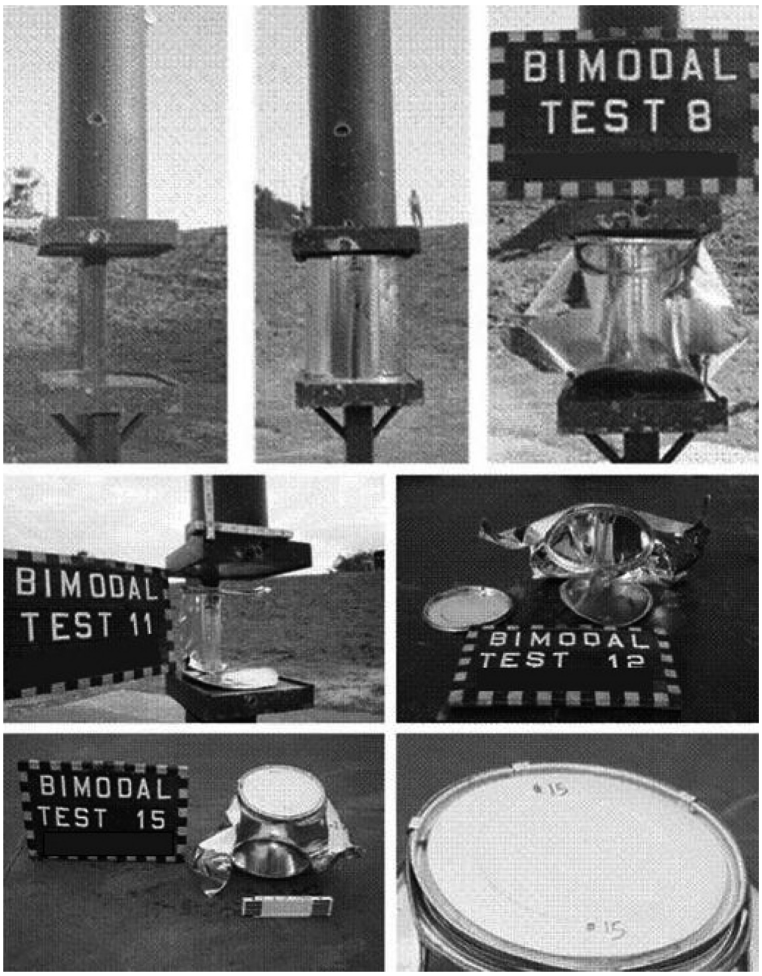

Fig. 3. Target structure and cans.

hydraulic ram would cause the ejected liquid and aerosol to be directed from the target can toward the charge (Fig. 2), a large fan was positioned behind the target along the line of sight from the target to the charge to blow the aerosol away and prevent it from settling onto the collection area. A fragment intercept was placed above the target can to shield the fan from possible high flying fragments. Fragment impact velocities were calculated using the recorded time of arrival data and the known distance between the aforementioned velocity break screens. Scoring the case fixes the dimensions of bomb fragments so the mass of a single fragment can be determined using the fragment volume times the density of the case material (steel or aluminum). The fragment energy input can then be calculated as the product of one-half the mass of a single fragment, the square of the fragment velocity and the number of fragment hits.

3. Test setup – Target cans

Target cans were 7.57 ℓ (2 gal) sized steel paint cans containing 7450 gm of water with 5% ullage. The cans were cylinder shaped and commercially manufactured with a 210 mm (8.25 in.) diameter, a total height of 241 mm (9.5 in.), and a thin wall thickness of 0.28 mm (0.011 in.). During the tests the cans were held in position by a rigid steel reaction mounting structure as shown in the upper left of Fig. 3. The ruptured can in the view in the upper right was replaced in the structure post-test for the photograph. Note that the structure restrains the can from moving

Table 1
Fragment properties

Fragment designation	Material type	Fragment thickness mm	Fragment height mm	Fragment width mm	Calculated fragment mass gm	Recovered fragment mass gm
SS	Steel	1.65	6.35	3.25	0.38	0.38*
AL	Aluminum	1.65	6.35	3.25	0.13	0.14*
LS	Steel	1.65	12.7	6.55	1.32	1.28*
XL2	Steel	5.00	15.2	15.2	9.26	6.68**
XL3	Steel	2.54	15.2	15.2	4.63	2.50**

*Based on 10 sample prescored fragments of each type torn along their score lines and weighed to determine their mean mass.
**Based on fragments found in soil posttest and weighed to determine mean mass.

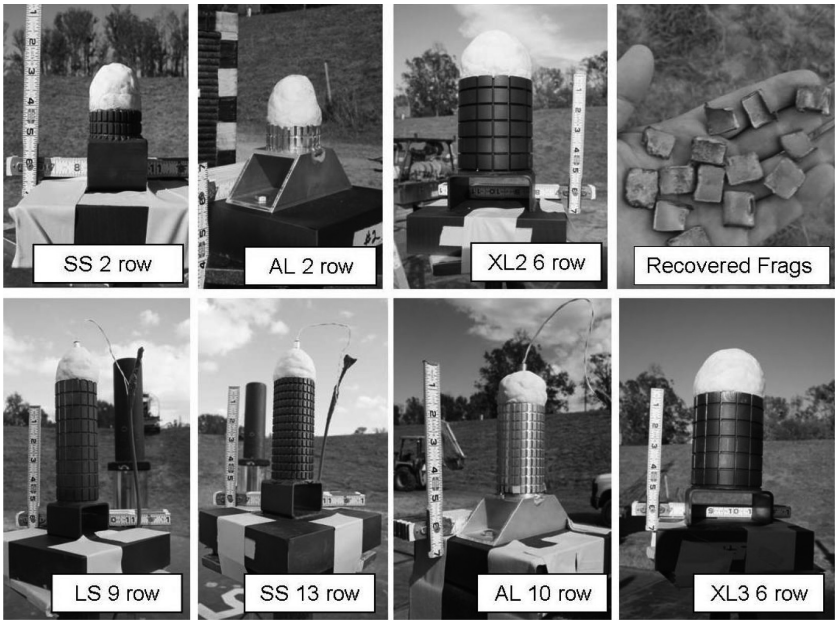

Fig. 4. Scored cased charges. Recovered XL2 fragments are shown.

away from the charge and keeps the lid and bottom of the can from deflecting vertically. This is a snug fit designed to produce a horizontal ejection of the liquid and an unimpaired deflection of the can sides. It does not necessarily hold a heavily damaged can in the structure following ejection of the liquid. In addition to the structure's vertical restraint, the can lids are held in place with six shipping clips. Lids cannot pop off easily.

4. Test setup – Scored charges

Table 1 lists the properties of individual fragments. The difference in the theoretical and recovered fragment masses indicates the release of fragments by detonation is different from a careful hand separation; however, no rigorous explanation for the magnitude of difference observed is offered. In the results presented later in this paper the mass determined from recovered fragments is used since they were the actual flying fragments. The charges were scored cylinders of aluminum or steel hand-packed with C4 explosive and capped with "domes" of C4 to produce a planar detonation wave entering the cylindrical casing. The seven different charges used for this test series are shown in Fig. 4. There were five different fragment sizes with charge casing lengths varied due to the number of fragment rows. The number of fragments designed to strike the target can was typically the row count less one, since all fragments had a similar and grouped trajectory except the top fragment. The recovered fragments shown in Fig. 4 are from an XL2 charge.

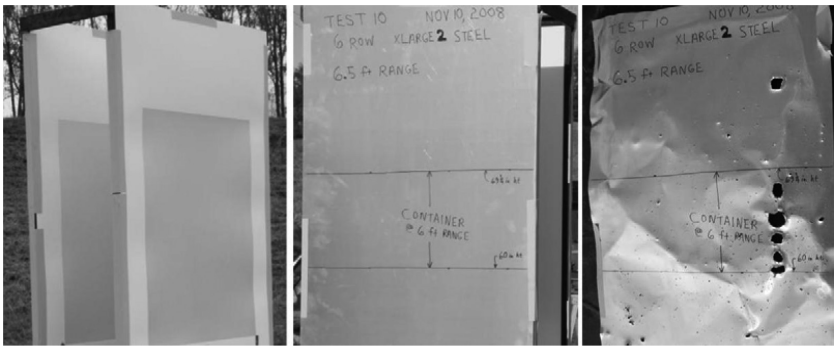

Fig. 5. Velocity screens and witness panel.

5. Test setup – Velocity measurement

Fragment velocities were determined using a pair of thin cardboard screens shown in Fig. 1 with a close-up shown on the left of Fig. 5. The surface of each screen holds a pattern of fine closely spaced parallel wire loops that acts as one of the resistors in a balanced electrical bridge circuit. When a fragment penetrates the screen it breaks the wire, unbalances the bridge and acts as a signal for the time of arrival of the fragment. Two such screens placed a known distance apart are used to determine the average velocity between screens. For this series new screens were placed one foot apart spanning and centered at the range of the target can for each test. The bomb to screen distance for the front screen was 1.68 m (5.5 ft), and for the rear screen it was 1.98 m (6.5 ft). The signal sampling rate was one megahertz. A thin aluminum witness plate was placed immediately behind the rear screen to physically record the fragment impact pattern for each test. The pattern should be the same as that which impacts the can, albeit the pattern is 1.27 to 1.90 cm ($1/2$ to $3/4$ in.) lower on the witness plate because of fragment drop over the additional 0.15 m (0.5 ft) in range. The pattern shown in Fig. 5 illustrates the directionality of a column of fragments as well as the high-strike behavior of the top row of fragments. This high-strike behavior is also evident in the upper left pictures of Fig. 3. Note the pattern on the witness plate was radially off center in this view as planned, due to using a common position to intercept multiple tests with different numbers of fragment columns.

6. Test setup – Fan wind speed

The airboat fan in Fig. 1 was used to ensure the aerosol did not settle on the collection surface. Table 2 shows the calibration data providing the fan winds generated in the vicinity of the target. Figure 2 shows a hydraulic ram from an earlier test series with the liquid/aerosol headed back toward the bomb. This was the expected behavior for this series. Therefore the fan was placed behind the target, blowing in the same direction as the central exiting velocity of the liquid and preserving symmetry blowing the aerosol off the collection area. To ensure the fan did not cause significant secondary evaporation, it was fitted with a remote control system. The fan was started just prior to the test and stabilized at 2000 rpm. It was cut off immediately after detonation and the wind speed quickly dropped to zero.

Figure 6 shows the settling velocity for 250 micron water particles in air to be 1.83 m/s (6 ft/s), and Table 2 shows the wind speed in the vicinity of the target to be about 32 km/hr (20 mph) or approximately 9 m/s (30 ft/s). Therefore, neglecting the initial velocity from the hydraulic ram and starting the settling from the target elevation, a 250 micron particle should be blown approximately 9 m (30 ft) from the target before falling to the ground. Since the water exiting velocity is in excess of 30.5 m/s (100 ft/s), even though it slows rapidly, it is probable that particles up to 300 microns were blown off the collection area. A further observation justifying the assumptions that the aerosol was carried away by the fan's wind, that the large droplets were not blown away, and that the non-aerosolized liquid was recovered is that the liquid fall-out patterns observed remained within the boundaries of the steel collection surface. Figure 7 shows the water fall-out pattern for Test 15 to be totally surrounded by dry areas of the recovery platform.

Table 2
Fan wind speed calibration

Airboat fan location	Range from container m	Direction from container	Height above test platform m	Wind speed (@ 2000 RPM) km/hr
On	3.0	NE	1.8	20
SouthEast	1.5	NE	1.8	26
Corner of	0.3	NE	1.8	34
Berm	0.3	SW	1.8	33
With	1.5	SW	1.8	29
Fan Prop	3.0	SW	1.8	24
25 m from	0.3	SW	2.7	27
Container	0.3	SW	2.4	31
	0.3	SW	2.1	31
	0.3	SW	1.8	32
	0.3	SW	1.5	31
	0.3	SW	1.2	32
	0.3	SW	0.9	37
	0.3	SW	0.6	34
	0.3	SW	0.3	31

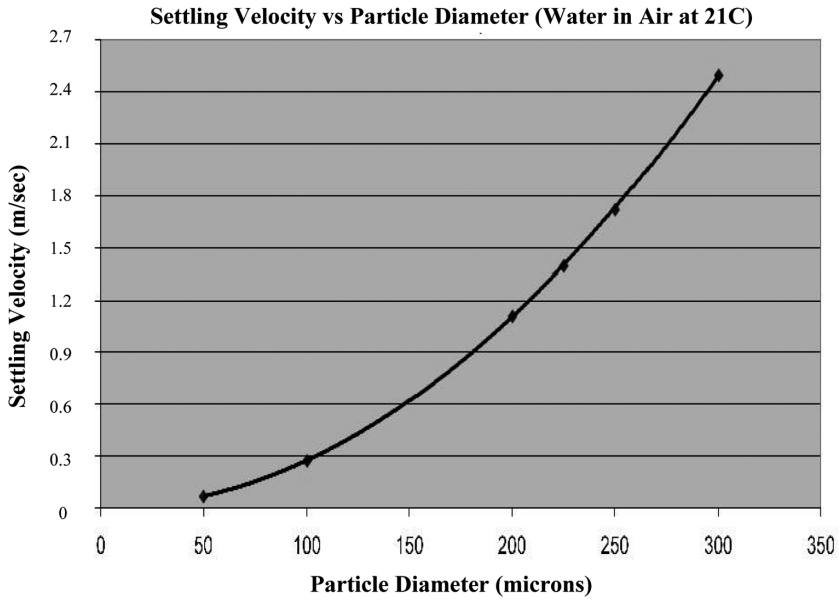

Fig. 6. Particle settling velocity.

7. Post-test – Liquid recovery

Liquid recovery was begun immediately after the blast and conducted quickly to minimize evaporation effects and was typically completed within 10 min of the blast event. The procedure was to scoop pooled liquid into a bucket and/or by mopping to absorb water with paper towels to dry the recovery platform. Any water remaining in the target can was added to the bucket and towel dried. All wet towels were placed in a plastic bag to prevent evaporation. All damp areas were mopped. After the bucket of water was weighed, bucket's tare weight was subtracted to provide the mass of water recovered in the bucket. The bag containing the recovery towels was weighed, and the tare weights of the towels and bag subtracted to give the mass of water recovered in towels. The two masses were summed to give the total mass of recovered water.

To calibrate the effectiveness of the recovery method, seven calibration tests were conducted by spilling known amounts of water. Four tests used different amounts of water (104 gm, 501 gm, 3,725 gm, or 7,450 gm) plus a repeat

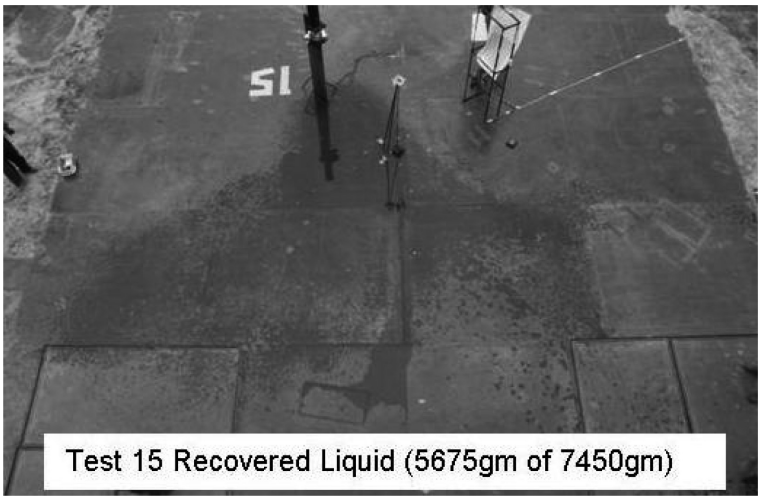

Fig. 7. Liquid pattern post-test 15.

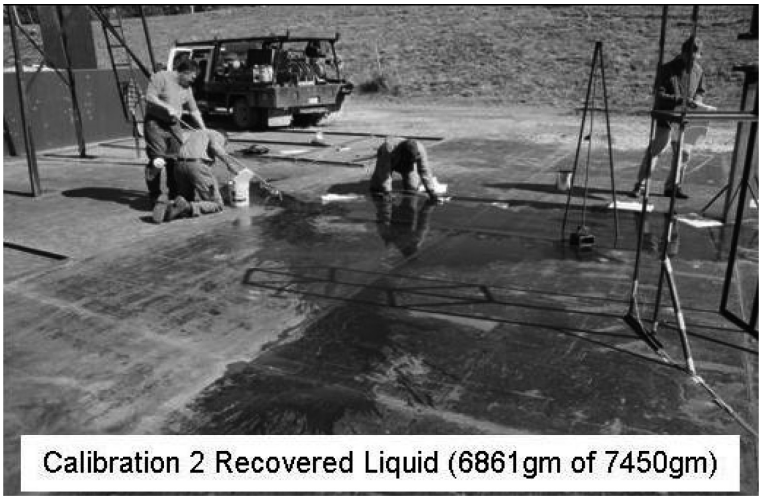

Fig. 8. Calibrating the recovery method.

test for three of these spillage amounts. The water was spilled or thrown onto the steel ground platform to simulate the dispersion patterns observed in the explosive tests. Figure 8 shows typical scooping and mopping efforts while recovering a test with 7,450 gm of spillage. All seven calibration tests spilled amounts, and recovered fractions are plotted in Fig. 9 along with a function fitted to this data. The calibration curve fit was subsequently used to adjust the recovered values for all 20 explosive tests. For all tests, including the calibration tests, the collection surface was cool to the touch, winds were calm to very light, fall temperatures were moderate, and humidity levels were similar. There was no evidence of excessive evaporation.

8. Summary of results

Results are summarized in Table 3 and Fig. 10. Additional information can be obtained from the experimental reports [1,2]. A plot of fragment energy deposited versus aerosolized fraction of the container's liquid is shown in Fig. 10. Figure 10 shows all the data points from this twenty test series, the linear model currently in use with its previous limited set of test data points, and the new recommended S-curve fit. The data points are plotted and

Table 3
Summary of results

Test No.	Recovered H2O mass		Missing	Fragment			Energy	Log	Aerosolized
	(Raw) gm	(Adjusted) gm	H2O gm	Type	Total mass gm	Velocity m/s	input J/kgm	energy input J/kgm	fraction
1	6208	6735	715	SS	0.764	1905	186.2	2.270	0.096
2	6632	7242	208	AL	0.144	2208	47.17	1.674	0.028
3	153	189	7261	XL2	26.72	2241	9012	3.955	0.975
4	620	744	6706	LS	10.21	2478	4209	3.624	0.900
5	3092	3394	4056	SS	4.584	2177	1459	3.164	0.544
6	4964	5343	2107	AL	1.296	1385	167.0	2.223	0.283
7	571	687	6763	XL3	12.50	2746	6329	3.801	0.908
8	5757	6215	1235	SS	1.146	2146	354.5	2.550	0.166
9	6662	7279	171	AL	0.288	1954	73.82	1.868	0.023
10	79	98	7352	XL2	33.40	2605	15,220	4.182	0.987
11	1474	1700	5750	LS	10.21	2292	3600	3.556	0.772
12	2799	3093	4357	SS	4584	2345	1692	3.228	0.585
13	6510	7094	356	AL	0.720	2032	199.6	2.300	0.048
14	1216	1418	6032	XL3	12.50	2381	4760	3.678	0.810
15	5675	6123	1327	SS	1.146	1893	275.8	2.441	0.178
16	6825	7450	0	AL	0.144	1693	27.73	1.443	0.000
17	292	357	7093	XL2	33.40	2849	18,200	4.260	0.952
18	1230	1434	6016	LS	10.21	2345	3768	3.576	0.808
19	2526	2811	4639	SS	4.584	2345	1692	3.228	0.623
20	5139	5532	1918	AL	1.008	1825	225.5	2.353	0.257

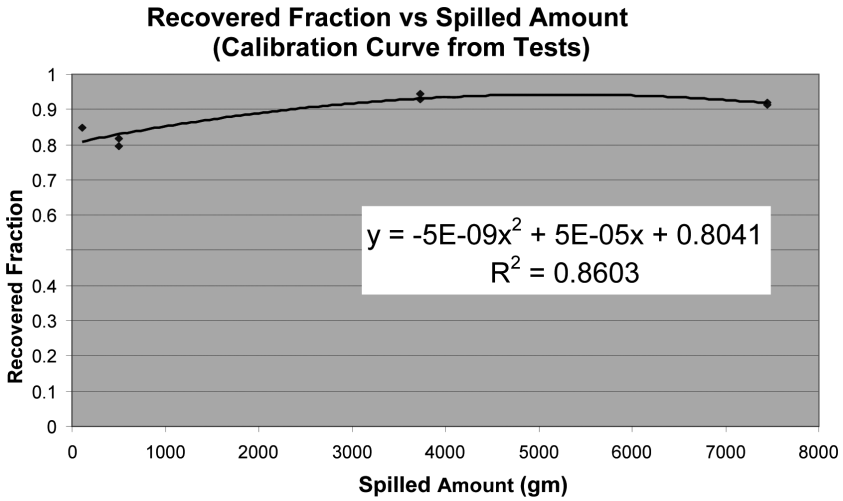

Fig. 9. Recovered liquid calibration.

numbered for each test to permit the reader to evaluate the scatter. For example, the velocity for Test 6 (Data Point 6) seems to be low. If it were the same as measured in the identical Test 20, the point would lie to the right of Point 20 and be much closer to the S-curve. While there is no hard evidence to exclude Point 6, the low velocity is suspect. What is evident is that all the data supports an S-curve that becomes asymptotic to zero at around 80 J/Kgm and asymptotic to 1 at around the FAE point of the linear model. It should be noted that 5 of the 6 previous data points (including the two full-scale DJ5 tests with much larger containers) on which the linear model rested support the new S-curve equally well. Also, a few of these previous data points used liquids other than water and a few tests were conducted at other test sites with generally less humidity. No other specific data are available for the previous data points other than the AF and fragment energy deposited values.

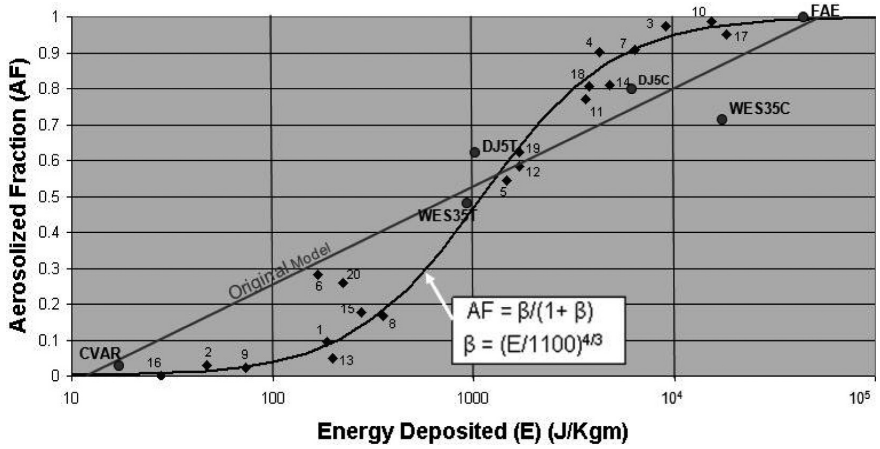

Fig. 10. Aerosolized fraction versus energy deposited.

9. Conclusion

The authors believe the new S-curve given above is a significant improvement, versus the current linear fit, to represent the relationship between the aerosolized fraction of water from a full tank of water impacted by bomb fragments and the impacting fragment energy per unit mass of water in the container. We further believe that reasonable extrapolations can be made to other liquids and larger containers. Our subsequent analyses suggest that points in the lower left portion of the graph represent conditions where the fragment/water interaction involves only a small portion of the water in the container, as would be the case for very large tanks. However, in this series we did not consider variables such as the container length to diameter ratio (L/D), the wall thickness of the container, liquids other than water, fragment shapes other than the thin rectangles shown in Fig. 4, and we treated the fragment energy expended in penetrating the container wall as negligible. Readers should make their own judgment with respect to the applicability of this data to specific problems.

Acknowledgements

This research was conducted by the U.S. Army Engineer Research and Development Center (ERDC), Geotechnical and Structures Laboratory (GSL), Vicksburg, MS, under the sponsorship of the Defense Threat Reduction Agency (DTRA). Technical guidance was provided to DTRA by Northrop Grumman Information Systems (NGIS) (now TASC Inc.) and Science Applications International Corporation (SAIC). Permission to publish this paper was granted by the Director GSL, DTRA and NGIS, and is gratefully acknowledged. NGIS approval for unlimited distribution is based on "22 CFR 125.4(b)(13) applicable (Log TASC-09-0363)". The authors thank the technical reviewers for their positive comments and recommendations for publication.

References

[1] P.W. Graham and E. Gayle, Albritton and Leo W. Stockham, Experimental Results for Bimodal Droplet Test Series, Draft Report, U.S. Army ERDC Vicksburg, MS and TASC Inc. Alb NM, 6 May 2009.

[2] P.W. Graham and E. Gayle, Albritton and Leo W. Stockham, Published date, 'Consequence Assessment Program, Experimental Results for Bimodal Droplet Test Series; Tests 1 through 20 and PT1," prepared for the Defense Threat Reduction Agency, Fort Belvoir, VA, prepared by U.S. Army Engineer Research and Development Center, Vicksburg, MS and TASC Inc., Alb, NM, Technical Report ERDC/GSL TR-10-42, September 2010.